Aerosol and Air Quality Research, 16: 1055–1066, 2016

ISSN: 1680-8584 print / 2071-1409 online
doi: 10.4209/aaqr.2015.02.0081

Particulate Pollution in the Sydney Region: Source Diagnostics and Synoptic Controls

Jagoda Crawford[1*], Alan Griffiths[1], David D. Cohen[1], Ningbo Jiang[2], Eduard Stelcer[1]

[1] *Australian Nuclear Science and Technology Organisation, Locked Bag 2001 Kirrawee DC NSW 2232, Australia*
[2] *Office of Environment and Heritage, NSW Department of Premier and Cabinet, Sydney, Australia*

ABSTRACT

Airborne particulate matter ($PM_{2.5}$) was sampled at Richmond and Liverpool, located in the Sydney Basin, Australia, and ion beam analysis was used to obtain the elemental composition. Using self-organising maps to classify synoptic weather systems, it was found that high $PM_{2.5}$ concentrations were associated with high pressure systems located to the east of the sampling sites. The highest median sulfur was associated with weak synoptic conditions and high soil dust days were more often associated with frontal systems.

To investigate the effect of local flows in the Sydney Basin, the Weather Research and Forecasting model (WRF) was used to generate meteorological data of 12 km resolution. A comparison was made between back trajectories generated using the higher-resolution WRF data, the 0.5° by 0.5° Climate Forecast System data and the 1° by 1° Global Data Assimilation System data. It was found that for high soil dust days, there were small differences between the different back trajectories. However, under weak synoptic conditions (high sulfur days), the back trajectories generated from higher resolution data showed larger variations over a 24 hr period. This was attributed to the meandering of local winds and sea-breezes.

Lower altitude back trajectories, generated from low resolution data, passed more often over the power stations located on the western side of the Great Dividing Range (while the sampling sites are on the east). This demonstrates the need for higher resolution meteorological data for generating low altitude back trajectories when the source and receptor are separated by hilly terrain.

In estimating the number of high sulfur days for which a power station was crossed, there was up to 20% difference at Liverpool and up to 10% difference at Richmond, between back trajectories starting at different altitudes and generated from meteorological data of three different resolutions.

Keywords: $PM_{2.5}$; Secondary sulfate; WRF; Back trajectory; SOM.

INTRODUCTION

Atmospheric particles (referred to here as particulate matter, PM) are an important trace component of the earth's atmosphere. PM plays a major role in the global radiative balance (e.g., Charlson *et al*., 1992; Hubert *et al*., 2003; Jiang *et al*., 2013b) and is detrimental to human health (e.g., Dockery *et al*., 1993; Moloi *et al*., 2002; Russell and Brunekreef, 2009). Because human activities represent a major source of PM, many administrations have developed policies with the aim of limiting the release of aerosols and precursor compounds (e.g., USEPA, 2007; NSW, 2011; VES, 2012).

The development of effective management strategies needs to be guided by an understanding of how much PM is emitted to the atmosphere, the activities which cause its emission, and the chemical and physical properties at release. It is also important to be able to anticipate the effect of processes acting on pollution in transit from the source to receptor. The concentration measured at a receptor can be significantly affected by the local meteorological conditions, chemical transformation in the atmosphere and prevailing synoptic weather systems (e.g., Davis and Gay 1993; Jiang *et al*., 2005). The association between synoptic weather systems and PM has been studied by a number of authors (e.g., Huang *et al*., 2009; Hawkins and Holland, 2010; Lai, 2014). Often an association has been reported between high PM and high pressure systems, which are themselves associated with low wind speeds and less pollutant dispersion. Lai (2014) linked high PM days at Taipei (Taiwan) with continental high-pressure systems. Huang *et al*. (2009) found that weak high pressure systems over mainland China lead

* Corresponding author.
Tel.: +61 2 9717 3885; Fax: +61 2 9717 9260
E-mail address: Jagoda.Crawford@ansto.gov.au

to high PM days at Hong Kong in winter and autumn, while typhoon episodes were responsible for most summer cases. Other authors that have found an association between high PM days and high pressure systems include Buchanan *et al*. (2002) and Lesniok *et al*. (2010). High pressure systems are, nonetheless, not the only systems to be associated with higher PM. Dayan and Levy (2005) reported that low pressure systems can also result in higher PM concentrations because strong winds can stir up such PM as soil dust.

In the Sydney region, links have been established between meteorology and overall air quality (e.g., Leighton and Spark, 1997; Hart *et al*., 2006; Jiang *et al*., 2013a). High ozone days are associated with high-pressure systems centred over the Tasman Sea, a ridge extending northwest across New South Wales and north-easterly sea-breezes. Low ozone days, in contrast, are associated with south-easterlies. High ozone days have been seen when troughs are present over east Australia with north-westerly to northerly flows affecting Sydney. Leighton and Spark (1997) found these synoptic conditions to have the highest occurrence of days with high pollution index (calculated using the O_3, NO_2, CO, SO_2, PM and visibility data).

Ongoing monitoring is necessary to quantify changing source strengths, and is especially valuable to assess the effectiveness of PM reduction strategies. The concentration and composition of aerosols can be monitored in near real time using mass spectrometry (Russell and Brunekreef, 2009; Hartonen *et al*., 2011), or, more commonly, by collecting samples on filters and then analyzing using off-line techniques (e.g., Ion Beam Analysis; Cohen 1996). The latter technique was used in this study.

To identify the major contributors to PM, back trajectories have been widely used to link source regions leading to high concentrations at a sampling site (e.g., Fleming *et al*., 2012; Liu *et al*., 2013). A large number of studies have used HYSPLIT (HYbrid Single-Particle Lagrangian Integrated Trajectory; Draxler and Rolph, 2003) with 1° by 1° meteorological data resolution (e.g., Park and Kim, 2004; Kim *et al*., 2005; Cohen *et al*., 2011). In two recent studies, for the Sydney region, back trajectories were generated using this methodology (Cohen *et al*., 2011, 2012). These studies were able to link high soil dust and sulfate days to possible source regions but the realism of the back trajectories was constrained by the low resolution meteorological data. It is not immediately clear that the conclusions of these earlier studies were affected by uncertainties in the trajectories, in part because the long integration time of the samples (24 hours) may have a masking effect.

Further complicating the issue is that the effect of low-resolution back trajectories might be source dependent. This is because the trajectory errors are likely to vary with synoptic conditions; concurrently different sources can be dominant under different synoptic conditions.

The aim of this study was to investigate the synoptic conditions leading to high particulate concentrations, and to understand the effect of increasing the meteorological data resolution on Lagrangian source diagnostics, in particular for 24 h particulate samples. We first used an unsupervised method to classify the Eastern Australian synoptic conditions. Then we used these classifications to identify the synoptic weather types which lead to high $PM_{2.5}$ (particulate matter with aerodynamic diameters of less than 2.5 μm) levels. We also used elemental concentrations to identify the conditions associated with high levels of soil dust (using Si concentrations) and secondary sulfate (using S concentrations). Conditions associated with high $PM_{2.5}$ concentrations are particularly important as research over the past two decades has shown that the greatest health risks from PM are associated with fine ($PM_{2.5}$) and ultrafine ($PM_{0.1}$) particles (e.g., Schwarts *et al*., 1996; Loomis, 2000). We then applied the source diagnostic method of Cohen *et al*. (2011, 2012) using both high- and low-resolution meteorological data fields. This method was applied to Si and S to test the importance of high-resolution meteorological fields under contrasting meteorological situations.

The remainder of this paper discusses the effect of high-resolution meteorology on the interpretation of $PM_{2.5}$ in the Sydney region. The Section on Sites and Methods describes the Sydney Basin and the sampling regime and then introduces the meteorological model used to generate the high-resolution meteorology, and the classification method, used to identify synoptic types. The back trajectories and source region diagnostic procedure is also described in the Section on Sites and Methods. This is followed by the presentation of the results of the synoptic classification and trajectory analysis and finally the conclusions.

SITES AND METHODS

Measurement Sites

$PM_{2.5}$ samples were collected at Liverpool; located at 33.925°S, 150.924°E, 20 m above sea level (asl); and Richmond; located at 33.618°S, 150.748°E, 19 m asl. Both sites are within the greater urban area of the Sydney basin (Fig. 1).

The Sydney basin is about 200 km north-south and 100 km east-west, bounded by the Great Dividing Range which rises to over 1000 m asl to the west. Smaller hills, 200 m asl, bound the basin to the north and south. Richmond is located near the north-western boundary of the basin; Liverpool is closer to the eastern side.

The basin is a natural trap for fine particle pollution generated locally (Cohen *et al*., 2011, 2012) or transported into the basin from sources outside of the basin (e.g., soil dust and secondary sulfate). In the winter months, inversions trap pollution in the basin, a situation sometimes associated with light westerly drainage flow. In the summer, sea breezes (which sweep pollution inland) are common near the coast.

Eight coal-fired power stations provide electricity to Sydney and the surrounding regions (Fig. 1). Their emissions are linked to high sulphur days in Sydney (Cohen *et al*., 2011). The Hunter Valley power stations (1, 2 and 3) are located at an altitude of ~200 m asl, those to the east (6, 7 and 8) are at ~15 m asl and those to the west (4 and 5) are on the western side of the Great Dividing Range, at ~900 m asl (Fig. 1).

Sample Collection and Analysis

At the Richmond and Liverpool sites, aerosols have

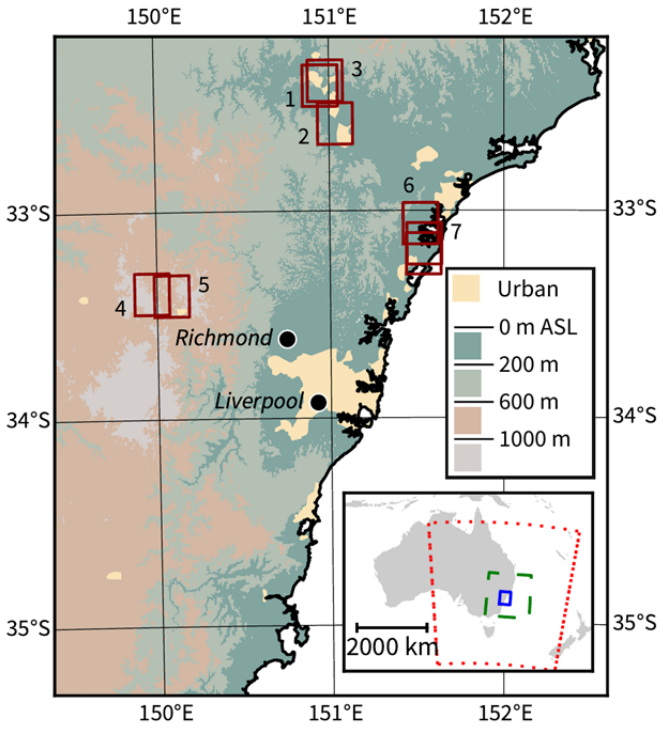

Fig. 1. Location of Richmond and Liverpool study sites, together with the coal fired power stations represented by numbered boxes. In the inset, the outer dotted box is the domain used in Fig. 2, the inner dashed box is the limit of the WRF domain and the solid box shows the limits of the detailed map. Map data from Geoscience Australia and the Bureau of Meteorology.

been sampled since 1998 using an IMPROVE $PM_{2.5}$ cyclone system with 25 mm diameter stretched Teflon filter at a typical flow rate of 22 L min^{-1} (Cohen *et al.*, 1996). Twenty-four-hour integrated samples (midnight to midnight) were collected twice a week (Wednesday and Sunday). In this study, observations between January 2007 and December 2013 were used, corresponding to the period for which the WRF simulations were available.

Elemental analysis of each aerosol sample was performed using accelerator-based ion beam analysis (IBA; Cohen *et al.*, 1996; Cohen *et al.*, 2004), which yielded elemental concentrations for 20 elements: H, Na, Al, Si, P, S, Cl, K, Ca, Ti, V, Cr, Mn, Fe, Co, Ni, Cu, Zn, Br, and Pb.

Aerosol source types can often be broadly characterised by their key elemental composition. For example, the five key elements commonly associated with soil dust are Al, Si, Ca, Ti and Fe (Begum *et al.*, 2011). K is often considered a marker for smoke, and S is an indicator of secondary sulfate, produced by the conversion of gaseous SO_2 to particulate sulfate in the presence of sunlight and water vapour (Seinfeld and Pandis, 1998). In this study we used Si as soil indicator and S as secondary sulfate indicator.

The Weather Research and Forecasting Model (WRF)

The WRF Advanced Research (WRF hereafter) model version 3.5.1 (Skamarock *et al.*, 2004; Skamarock and Klemp, 2008) was used to carry out dynamical downscaling. The main advantage of downscaling, compared with using the low resolution data directly, is that processes which are at a subgrid-scale in the global model can be simulated explicitly in the regional model. If these processes are simulated accurately, back trajectories will also be more accurate. This advantage needs to be balanced against the computational effort and the need to verify the results.

The WRF simulations were carried out using a configuration similar to the pollution transport simulations of Angevine *et al.* (2013), with a horizontal resolution of 12 km, temporal resolution of 1 hour and 50 vertical levels. The sensitivity of back trajectories to the temporal and spatial resolution of meteorological data is discussed in Draxler (1987). The temporal resolution is likely to have had an impact on trajectories, but the necessary temporal resolution increases with the horizontal resolution (Bowman *et al.*, 2013).

More details of the WRF simulations are presented in the Supplementary Information.

Self-Organising Map (SOM) Classification

In this study, a synoptic type classification was derived through a two-phase batch SOM classification procedure (CP2) detailed in Jiang *et al.* (2012, 2014). The SOM (Kohonen, 2001) is an unsupervised method for data classification and visualisation. An important property of the SOM is that nodes in the output space are arranged so that similar nodes are close to each other and dissimilar nodes further apart (Jiang *et al.*, 2013a). A description of how the CP2 procedure was applied to synoptic charts is presented in the Supplementary Information.

Source Regions

Two source types were considered, namely wind-blown soil dust (indicated by Si) and secondary sulfate (indicated by S). Based on the locations of known sources, back trajectories were used to link measured $PM_{2.5}$ with potential emissions from these sources. Cohen *et al*. (2011) identified the possible source regions for long-range transport of soil dust contributing to measurements at the Liverpool site. Of the soil source regions identified in Cohen *et al*. (2011), the Riverina agricultural region (located at 34.7°S and 146.5°E) was the only region located in the domain considered under WRF (Fig.1). The desert regions are situated outside of the WRF domain and thus were not considered in this study. As in Cohen *et al*. (2012), the effects of eight power stations (which may contribute to secondary sulfate; Fig. 1 and Supplementary Table 3) were considered in this study for both the Richmond and Liverpool sites. It is important to note that, while there may be sources other than the power stations contributing to secondary sulfate, the scope of our diagnostic was limited to determining the proportion of high sulfate days on which air masses passed over the power stations before arriving at the sampling sites. In particular, we were interested in how the conclusions might change when using the higher-resolution WRF meteorological data.

As in Cohen *et al*. (2011, 2012), the source regions were represented by rectangles. If a back trajectory passed over the rectangle before arriving at the measurement site, it was considered that the source region (rectangle) contributed to the measurement at the sampling site. The number of source region crossings was counted based on:

(1) the 1° by 1° GDAS meteorological data (referred to as the GDAS back trajectories hereafter);
(2) the 0.5° by 0.5° CFS meteorological data, i.e., the WRF boundary conditions (referred to as the CFS back trajectories hereafter); and
(3) the 12 km by 12 km meteorological data generated using WRF (referred to as the WRF back trajectories hereafter).

The defined rectangles for the power stations are given in Supplementary Table 3. The Riverina was defined at latitude –34.7° ± 0.6° and longitude 147.1° ± 1.1°.

The high soil dust days and high secondary sulfate days were chosen to be those in the top 10% of Si and S, respectively. As a result, samples with Si greater than 131 ng m^{-3} at Richmond and 176 ng m^{-3} at Liverpool were considered for counting the number of back trajectory crossings over the Riverina agricultural region. Samples with S greater than 693 ng m^{-3} at Richmond and 761 ng m^{-3} at Liverpool were considered for back trajectory crossings over the power stations. This selection resulted in 64 samples for Richmond and 72 samples for Liverpool.

Back Trajectories

Air mass back trajectories were calculated using HYSPLIT. As a baseline case, similar to many previous studies, back trajectories were calculated using meteorological data of 1° × 1° horizontal resolution and 23 vertical levels generated by the global data assimilation system (GDAS/GFS). The GDAS model is routinely run by the National Weather Service's National Centre for Environmental Prediction (NCEP) and the data files are available at ftp://arlftp.arlhq.noaa.gov/archives/gdas1. A temporal resolution of 3 hours is achieved by combining the analyses (every six hours from GDAS) with three hour forecasts from GFS.

We also generated back trajectories using the NCEP CFS data and the WRF-generated high-resolution meteorological data. In particular, CFS data are outputs from coupled NCEP atmospheric and ocean models. The CFS analysis runs every six hours and is available in near real time (Saha *et al*., 2013). We also used data from the closely-related CFS Reanalysis (CFSR), available from 1979–2011 (Saha *et al*., 2010), to completely cover our study period. The atmospheric model in CFS/CRSR has a horizontal resolution of around 38 km and 64 hybrid levels; however the data for forcing HYSPLIT are archived at 0.5 degrees on 37 vertical pressure levels.

For each of the meteorological drivers, five day back trajectories were calculated with a starting altitude of 300, 500 and 800 m above ground level (agl). These altitudes were chosen so that the receptor was typically below the top of the daytime boundary layer. More than one height was considered as a simple way of assessing the sensitivity to starting altitude. Trajectories were generated for each hour of each day for which the aerosol samplers were operating, i.e., 24 back trajectories were generated for each day.

When meteorological data of different resolution is considered, it is expected that the back trajectories would exhibit a spatial variation and hence the number of back trajectories crossing over the source defining rectangles might change. This is examined in the Sections labelled; Trajectories for High Sulfur Days and Trajectories for High Soil Days.

RESULTS AND DISCUSSIONS

Self-Organising Map (SOM) Classification

The SOM classification for eastern Australia is presented in Fig. 2, the average wind directions for each synoptic type are presented in Fig. 3, and the frequency of occurrence (percentage) by season is shown in Table 1. The resulting classification consisted of 20 types/nodes arranged in 5 rows and 4 columns, similar to Jiang *et al*. (2014). Similar systems appear close together in the output space. Westerly troughs are mapped onto the nodes in the top-left corner and were more frequent in winter and spring. Easterly troughs are mapped to the top-right corner and were more frequent in summer. Continental high pressure systems are mapped to the bottom-left and were more frequent in winter. Tasman highs are mapped to nodes in the bottom-right. The nodes with the most frequent occurrence were 16, 5, 1, 20 and 18 with 7.9, 7.6, 7.1, 7.0 and 6.5% of occurrences, respectively. Nodes with the lowest frequency of occurrence were the transition types in the middle of the SOM plane (i.e., nodes 8, 13, 12, 7, 14 and 9 with 3.6, 3.5, 3.2, 3.0, 2.9 and 2.5%, occurrence, respectively). The mean streamlines (Fig. 3) illustrate interactions between prevailing synoptic flows and local circulation features (e.g., sea breezes). These results agree well with Jiang *et al*. (2013a) and Jiang *et al*. (2014).

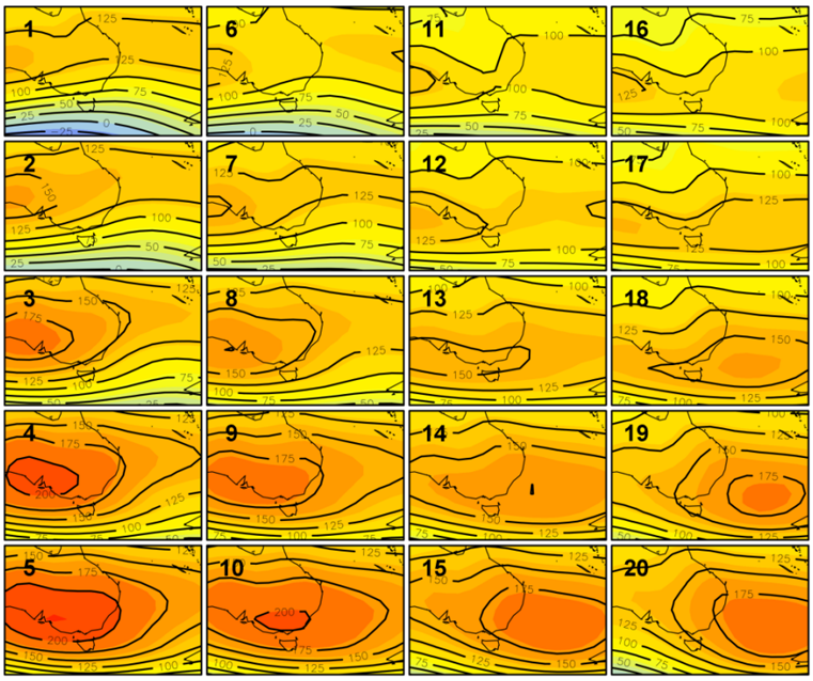

Fig. 2. The mean geopotential height maps of 20 synoptic types on the SOM plane. Contour interval: 25 m. Type id numbering from 1 to 12 is in large black font. The colour scale is used to highlight low (blue) to high (red) values in online version.

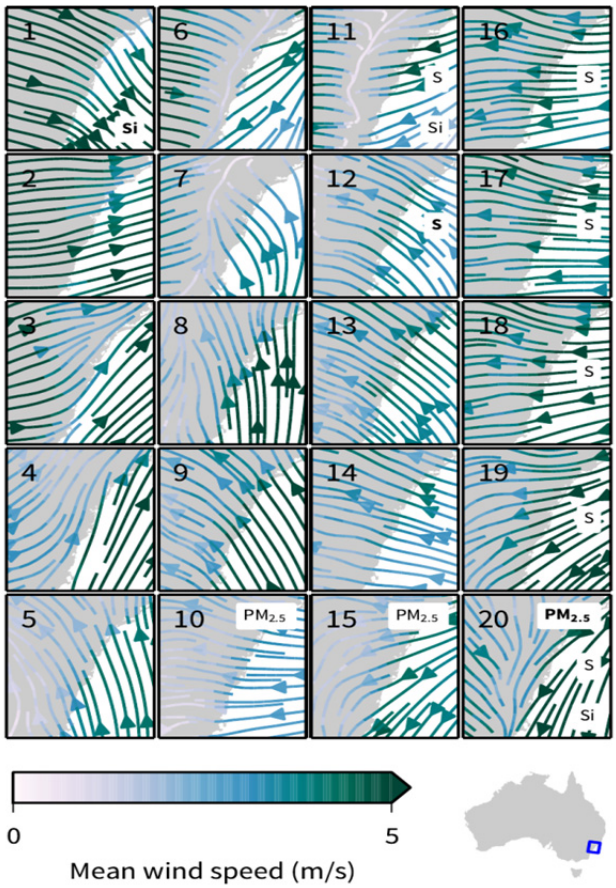

Fig. 3. Mean streamlines in the Sydney region 10 m AGL at 0600 UTC (1600 LST) corresponding to each synoptic type, generated by the WRF simulation. The symbols $PM_{2.5}$, S, and Si indicate synoptic types where the corresponding measurements were high with the highest synoptic type shown in bold (details in Figs. 4, 5, and 6).

Table 1. Average days in year (a) and conditional frequencies (b)–(e) of synoptic types in four austral seasons on the SOM grid corresponding to Fig. 2. Conditional frequency values are calculated as the percentage of days in each season over all days allocated to a given synoptic type.

a. Annual			
26	14	18	25
17	9	10	21
23	14	13	23
21	10	14	20
31	16	17	25

b. Summer (Dec–Feb)				c. Autumn (Mar–May)			
3.13	34.78	69.44	81.96	13.53	16.32	10.64	10.37
1.34	19.02	48.90	71.67	19.28	28.21	22.44	20.19
0.60	6.65	26.84	52.71	21.93	45.78	42.80	32.62
0.05	2.59	9.08	25.29	22.79	46.17	51.75	39.92
0.03	0.29	1.80	4.42	22.19	32.10	31.78	23.52
d. Winter (Jun–Aug)				e. Spring (Sep–Nov)			
39.84	9.38	1.58	0.22	43.49	39.52	18.35	7.46
43.29	13.50	3.11	0.52	36.09	39.27	25.55	7.62
50.47	18.64	4.71	0.78	26.99	28.92	25.65	13.89
56.44	26.92	12.25	3.48	20.71	24.33	26.92	31.30
63.76	47.15	38.57	35.07	14.02	20.46	27.85	36.99

$PM_{2.5}$ by Synoptic Type

Box and whisker plots of $PM_{2.5}$ concentrations, grouped by synoptic type, are presented in Fig. 4. The highest median concentration of $PM_{2.5}$ was seen for synoptic type 20, at both sites. For this synoptic type a high pressure system was located south-east of Australia centred over the southern Tasman Sea with a northerly gradient flow over coastal New South Wales (Fig. 3). The next highest median $PM_{2.5}$ was seen for synoptic types 15 and 10, once again associated with high pressure systems and occurred more often in autumn and winter. This finding is consistent with findings in other parts of the world, where high PM concentrations have been associated with high pressure systems (e.g., Buchanan *et al*., 2002; Huang *et al*., 2009; Lesniok *et al*., 2010; Lai 2014), and previous studies for the Sydney region (using a pollution index; Leighton and Spark, 1997). However, low $PM_{2.5}$ concentrations corresponded to the Tasman high pressure synoptic types 18 and 19. Unlike synoptic type 20, where the gradient wind was north-westerly and opposed by the sea breeze, the high pressure system in synoptic types 18 and 19 resulted in steady north-easterly flow.

Sulfur (S) by Synoptic Type

Box and whisker plots of S concentrations, grouped by synoptic type, are presented in Fig. 5. The highest median S concentration at both sites was recorded for synoptic type 12. High concentrations of sulfur were also recorded for synoptic types 11 and 17 which were also characterised by weak synoptic conditions with troughs over eastern Australia and to the west of the Great Dividing Range. The other group of high sulfur concentrations were synoptic types 18 to 20, for which a high pressure system appeared south-east of Australia. Most of these synoptic types occurred more often in the warmer months of the year (Table 2) and were associated with easterly or north-easterly flow conditions in the whole region or over the coastal areas (Fig. 3). The seasonal bias in synoptic type frequency makes interpretation less straightforward because, in summer, more sunlight favours the conversion of SO_2 to particulate sulfate. Nevertheless, the synoptic patterns are also important since the weak synoptic forcing associated with these types also favours low rates of pollution dispersion. The lowest S concentrations were seen for synoptic types 1 to 5, which occurred more often in winter and also corresponded to the opposite wind direction: southerly or westerly flows.

In summary, high sulphur days were associated with weak synoptic conditions, occurring most often in summer. This was due to reduced pollution dispersion in the study region and favourable conditions for chemical reactions.

Si by Synoptic Type

Box and whisker plots of Si, grouped by synoptic types, are presented in Fig. 6. The highest Si was recorded for synoptic type 1, characterised by the passing of a cold front over South Australia. Synoptic type 1 was most prevalent in spring and winter, and was characterised by strong synoptic pressure gradients (Fig. 2) with high-speed westerly winds prevailing across the Sydney basin (Fig. 3).

Dust storms, which erode soil from the continental interior, occur during west to east passage of frontal systems (McTanish *et al*., 2005). These storms are most common between September and December. Synoptic type 1 closely approximates the synoptic conditions which led to the dust storm on 23 October, 2002 (McTainsh *et al*., 2005). Storms, like this one, transport dust from distant sources into the Sydney region (e.g., Cohen *et al*., 2011). High Si was also recorded at both Richmond and Liverpool for synoptic types 11 and 20, but these were more likely to be from sources within the basin.

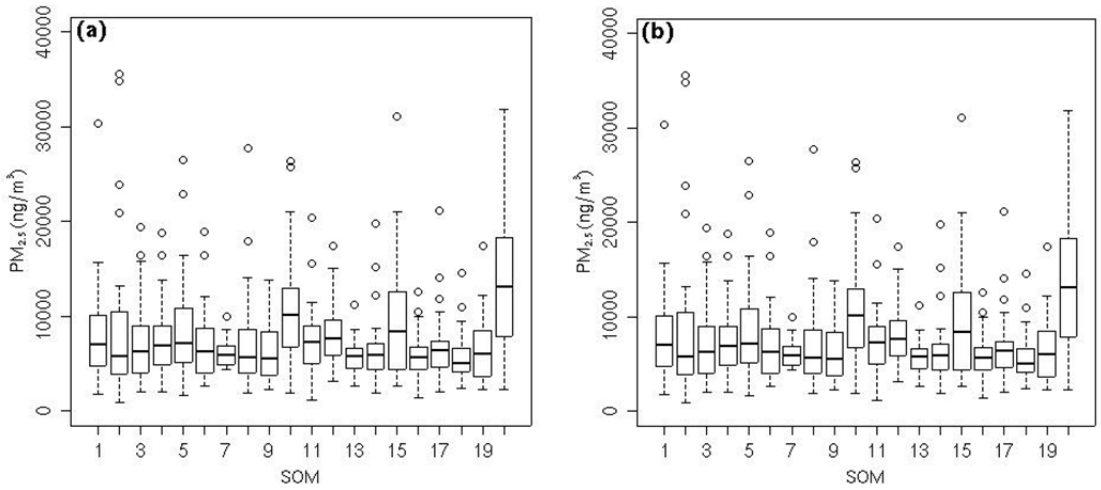

Fig. 4. Box and whisker plots of $PM_{2.5}$ concentrations by synoptic type at (a) Richmond and (b) Liverpool. Boxes represent the 25th and 75th percentiles, the median is represented by the line through the box, whiskers represent the 10th and 90th percentiles and extreme events are indicated by open circles.

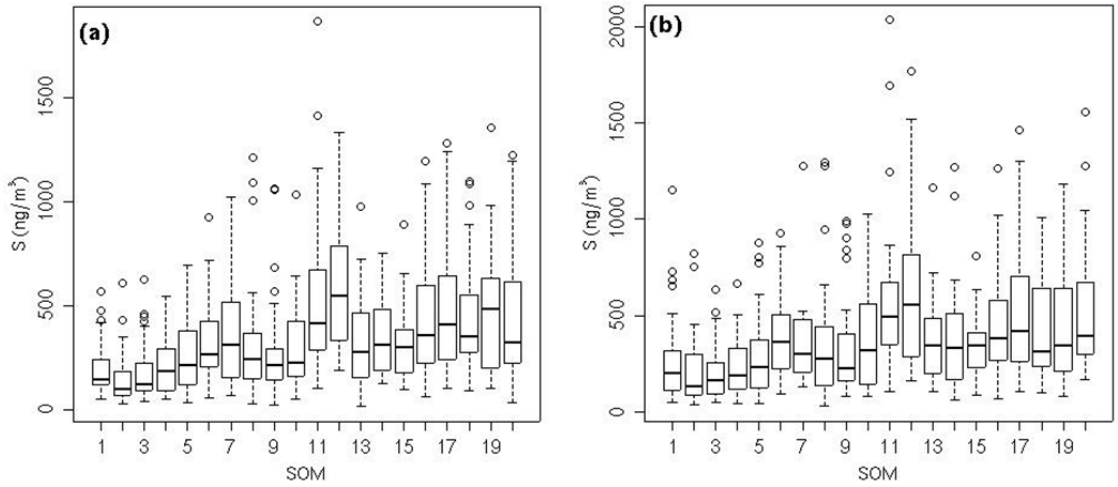

Fig. 5. Box and whisker plots of S concentrations by synoptic type for (a) Richmond and (b) Liverpool. Boxes and whiskers as for Fig. 4.

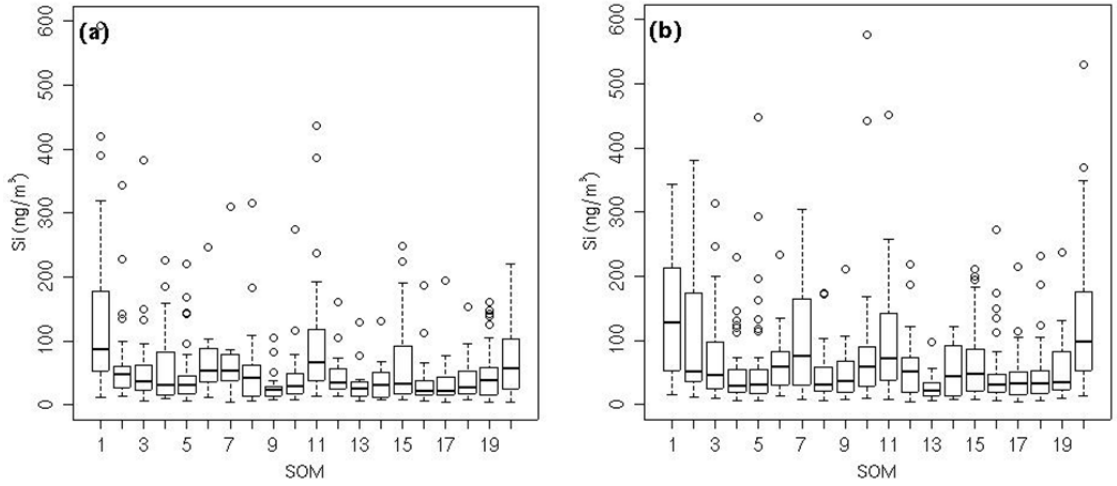

Fig. 6. Box and whisker plots of Si concentrations by synoptic type for (a) Richmond and (b) Liverpool. Boxes and whiskers, as in Fig. 4.

Trajectories for High Sulfur Days (Top 10% of S)

Back trajectory behaviour and the number of crossing with the rectangles, representing power stations, for the top 10% of sulfur days, are presented in this section.

Of the 64 days with high sulfur samples at Richmond, 56 fell into the warm months (October–March), when meteorological conditions were more favourable for the conversion of SO_2 to particulate sulfate. Most of these samples were classified into two synoptic groups, types 11 and 12, and types 17 to 20. Of the 72 days with high sulfur samples at Liverpool, 58 occurred in the warm months. From back trajectory analysis, the majority of samples were associated with north-easterly winds, travelling west and then turning to north-westerly before arriving at the sampling sites (Fig. 7). However, depending on the meteorological forcing, there were differences in back trajectories. For back trajectories at 300 m, some of the WRF back trajectories did not travel west to the extent the GDAS back trajectories did. An example is shown in Fig. 7, taken from the 28 August 2011. On this day, there were 7 GDAS back trajectories, 4 CFS back trajectories and only 3 WRF back trajectories crossing Mount Piper. The differences in these trajectories would be due to the wind fields used by the HYSPLIT model for trajectory calculations. The WRF simulation, due to the higher resolution of the topography, would produce a better representation of the wind field. A difference of several hundred meters was seen in the local terrain between the GDAS and WRF topography representation. For example, the altitude of Richmond (located at 19 m asl) was defined as 266 m asl in GDAS but 83 m asl in the WRF terrain. At a point 0.75° west of Richmond, the GDAS terrain was 679 m asl, whereas the WRF terrain altitude was 860 m asl. Hence, the higher terrain in the WRF simulation might have prevented air parcels from travelling further west across the Great Dividing Range, with implications for inferences about potential sources. See for example the back trajectories in bold in Fig. 7; the WRF back trajectories appear to have been blocked from travelling west.

For back trajectories starting at altitude of 300 m (agl), there were about twice the number of crossings over the power stations at Mount Piper and Wallerawang (located on the western side of the Great Dividing Range) under the GDAS data, compared to that under the CFS and WRF data (Tables 2 and 3). This difference is further illustrated in Section 4 of the Supplementary Information. The difference of crossings between the GDAS and WRF data was smaller for trajectories starting at higher altitude. For back trajectories at 800 m agl, a difference of 26% was seen for Mount Piper at Richmond and 14% at Liverpool, indicating that the terrain influence was less for back trajectories starting at higher levels.

The average wind speed for high S days (Tables 2 and 3) was generally lower than that for high Si days (Tables 4 and 5; which will be discussed in the Section; Trajectories for High Soil Days). During periods of weak synoptic forcing, e.g., under synoptic types 11 and 12; the mesoscale features (such as sea breezes) become relatively more influential on the trajectory directions. When forced with the WRF output, which resolves smaller scale features compared to the coarser GDAS data, the 24 back trajectories were generally more diverse (i.e., a larger path domain) than those driven by the GDAS data. Consistently, there were fewer high sulfur days with no back trajectory crossing over the power stations for the WRF data.

In summary, across the meteorological data of different resolution and the varying starting heights of the back trajectories, there were between 49 and 62 days out of the total high sulfur days (72 days) for which a back trajectory had passed over a power station before arriving at Liverpool. At Richmond, there were between 52 and 58 days out of

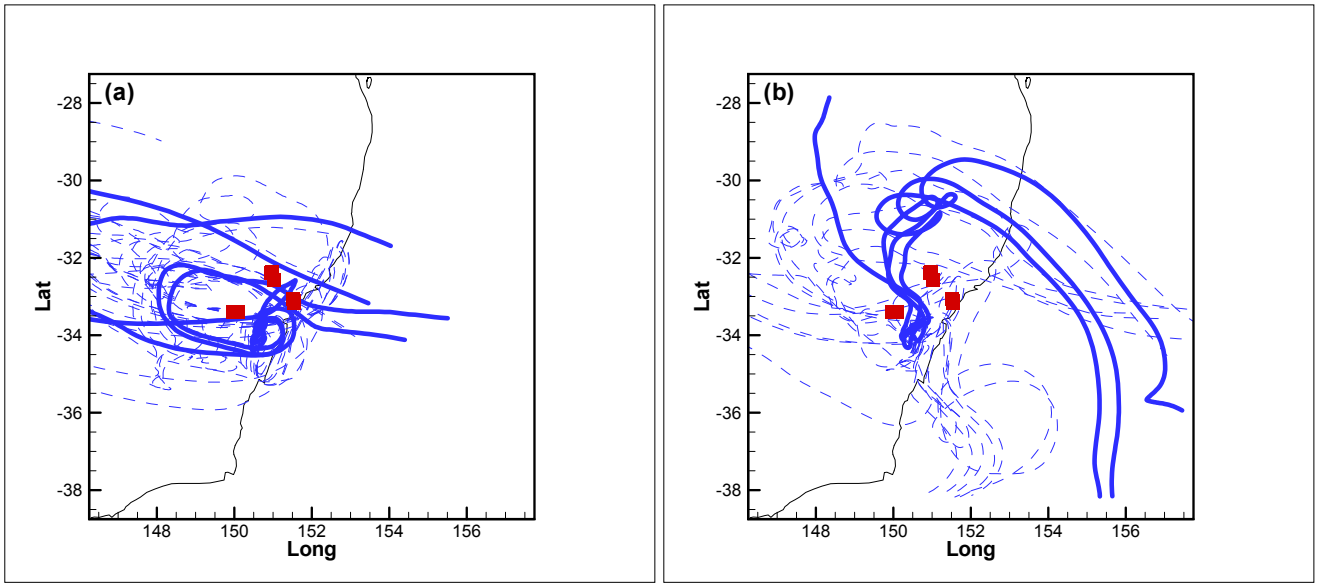

Fig. 7. Difference between GDAS (left) and WRF (right) back trajectories for 28/8/2011, arriving at 300 m agl, at Richmond. The red squares are the power stations. Mount Piper located to the west, had 7 back trajectories crossing under GDAS, 4 under CFS (not presented) and 3 under WRF.

Table 2. Number of back trajectory crossings with the power stations for the GDAS, CFS and WRF back trajectories starting at various heights at Richmond. The wind speed is the average of the wind speeds at the sampling site.

	300 m			500 m			800 m		
	GDAS	CFS	WRF	GDAS	CFS	WRF	GDAS	CFS	WRF
Bayswater	65	56	67	51	65	83	80	85	90
Liddell	66	59	63	49	66	84	79	86	87
Redbank	88	62	93	69	75	107	81	103	105
Eraring	175	196	174	123	186	147	151	200	170
Vales Point B	168	191	173	125	165	149	132	187	168
Munmorah	169	199	168	123	172	147	147	195	176
Mount Piper	89	55	49	82	50	45	96	101	71
Wallerwang	100	69	60	100	65	59	98	120	80
Total	920	887	847	722	844	821	864	1077	947
Wind speed (m s^{-1})	4.28	4.81	5.69	8.89	8.18	5.86	4.74	4.81	5.29
Days with no crossing	11	10	10	10	12	7	12	7	6

Table 3. Number of back trajectory crossings with the power stations for the GDAS, CFS and WRF back trajectories starting at various heights at Liverpool. The wind speed is the average of the wind speeds at the sampling site.

	300 m			500 m			800 m		
	GDAS	CFS	WRF	GDAS	CFS	WRF	GDAS	CFS	WRF
Bayswater	59	52	71	50	37	58	46	76	63
Liddell	53	49	70	53	43	59	45	79	60
Redbank	68	63	78	65	63	80	60	58	78
Eraring	149	198	188	158	202	174	138	169	141
Vales Point B	163	200	202	169	204	168	146	170	140
Munmorah	154	201	192	167	199	166	136	171	142
Mount Piper	75	43	36	57	87	48	93	104	80
Wallerwang	80	46	39	65	82	56	93	106	94
Total	801	852	876	784	917	809	757	933	798
Average wind speed (m s^{-1})	4.47	4.39	6.32	4.84	4.96	6.29	5.13	5.19	5.58
Days with no crossing	23	21	18	19	16	14	19	16	10

Table 4. Number of back trajectory crossings with the Riverina soil region for the GDAS, CFS and WRF back trajectories starting at various heights at Richmond. The wind speed is the average of the wind speeds at the sampling site.

	300 m			500 m			800 m		
	GDAS	CFS	WRF	GDAS	CFS	WRF	GDAS	CFS	WRF
Riverina crossings	404	364	413	431	386	388	496	403	401
Average wind speed (m s^{-1})	6.76	6.59	8.3	8.53	8.4	9.17	10.58	8.93	9.21

Table 5. Number of back trajectory crossings with the Riverina soil region for the GDAS, CFS and WRF back trajectories starting at various heights at Liverpool. The wind speed is the average of the wind speeds at the sampling site.

	300 m			500 m			800 m		
	GDAS	CFS	WRF	GDAS	CFS	WRF	GDAS	CFS	WRF
Riverina crossings	543	496	493	577	490	474	614	569	473
Average wind speed (m s^{-1})	6.34	6.15	8.08	10.12	7.34	8.63	16	8.29	8.5

the total (64 days) passing over a power station. One of the contributing factors to the lower number of crossings with power stations at Liverpool under the GDAS and CFS data was due to its location further south and closer to the coast (than Richmond). The Liverpool back trajectories, associated with coastal and off-shore high pressure systems, passed over the power stations less frequently. Generally, under WRF there was a larger variation in the path covered by the 24 back trajectories on a given day (see for example Fig. 8, where the WRF back trajectories show higher variation). Another contributing factor was that the sea-breeze effect was better represented under the WRF generated data, resulting in more meandering in the trajectories (e.g., those shown by Fig. 2 in the Supplementary Information, where the sea breeze effect is seen in the WRF back trajectories).

Trajectories for High Soil Days (Top 10% of Si)

In contrast to sulfur, wind erosion and soil uplift occurs

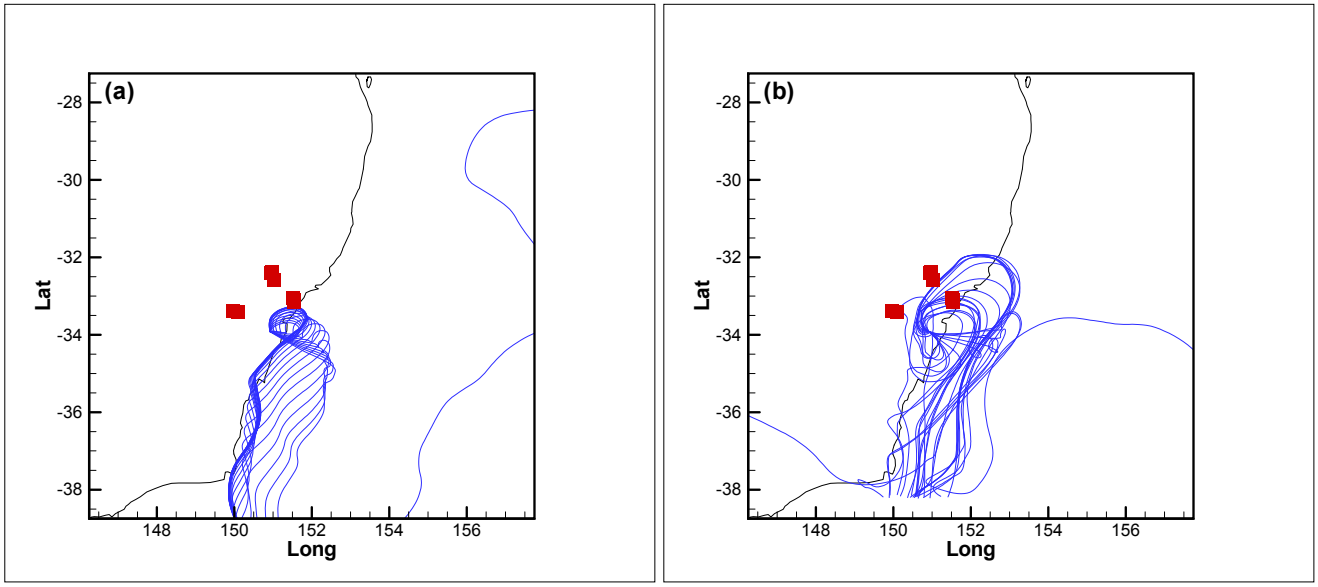

Fig. 8. Difference between GDAS (left) and WRF (right) back trajectories for 22/4/2007, arriving at 300 m agl, at Liverpool. The red squares are the power stations.

under conditions of higher wind speeds. As shown earlier, most of the high soil days were classified into synoptic types 1, 11 and 20. The largest number of high Si samples occurred in September and October – a well-known period of dust storms (McTainsh *et al.*, 2005). The differences between back trajectories generated with the GDAS, CFS and WRF data are investigated in this section, and in particular for defining the number of crossings with the Riverina rectangle.

The average wind speeds of back trajectories and number of back trajectory crossings with the Riverina region are shown in Tables 4 and 5 for Richmond and Liverpool, respectively. In all cases, the average wind speeds were above 6.15 m s^{-1}, considerably higher than the average wind speeds corresponding to high sulfur days.

There was little difference in the number of individual crossings with the rectangle representing the Riverina agricultural region for back trajectories starting at an altitude of 300 m agl (Tables 4 and 5). The difference increased with the staring altitude (with the GDAS back trajectories arriving at 800 m agl showing a greater variation on a given day). However, the difference was less significant compared to the difference seen for the high S days. It is notable that for trajectories starting at 800 m agl, the average wind speeds at Liverpool for the GDAS data were higher than that for the WRF or CFS data. A closer examination of the GDAS data showed that there were 5 days with wind speeds greater than 30 m s^{-1} with the median of wind speeds for the remaining days being ~10 m s^{-1}.

Overall, the differences between the GDAS, CFS and WRF back trajectories were small for the high soil days. The difference diminished further if we did not count the number of crossings on a given day, but were only interested in whether a crossing had occurred on a given day.

In summary, the results from this study show that when associating measurements at a receptor location with source regions, the meteorological data resolution is more important for weak synoptic conditions.

CONCLUSION

In the Sydney region, as for other parts of the world, high $PM_{2.5}$ days were associated with high pressure systems. Overall, a strong association was seen between observed $PM_{2.5}$ and synoptic types. Like $PM_{2.5}$ concentration, the occurrence of synoptic types was season-dependent, which contributed to the strength of this association. When elemental composition was considered, the highest median sulfur was associated with weak synoptic conditions, whereas the highest silicon was more often associated with frontal systems (associated with higher wind speeds), as was also observed in other parts of the world.

Back-trajectories were used to link the highest $PM_{2.5}$ days with known source regions. While most previous studies have used coarse resolution data, in this study we investigated the back trajectory sensitivity when using meteorological data of different resolution (1 degree versus 12 km).The results show that when using the lower resolution meteorological data, back trajectories starting at low altitude were more likely to cross the Great Dividing Range. This led to a different interpretation of the measured sulfur, implying a stronger contribution to sulfur from the Mount Piper power station. This finding demonstrates that, for studies in complex terrains, the resolution of the terrain is important, particularly when considering back trajectories arriving at lower altitude.

Under high sulfur days there was more difference between the 24 WRF back trajectories for a given day than for the corresponding GDAS back trajectories due to the effect of meandering of local winds and sea-breezes under synoptic conditions associated with high sufur days. The difference was less for high soil days, which occur on days with strong

synoptic-scale winds with less influence from small-scale features. This finding indicates that when considering sources that are higher under weak synoptic conditions, higher resolution meteorological data is of benefit whereas for those sources that are higher under the influence of strong synoptic conditions (e.g., fronts) the resolution in data is less critical.

When estimating the number of high sulphur days that had a contribution from the power stations, there was a relatively small difference of up to a maximum of 20%. Thus, the conclusions of Cohen *et al*. (2011, 2012) are largely unaffected by trajectory errors, despite using low-resolution meteorological data. The difference in the number of crossing with source region, for back trajectories generated by the different meteorological data resolution, was small as the sampling was undertaken over a 24 h period and then 24 back trajectories were generated for each day resulting in the coverage of a larger geographic region. We expect that the advantage of using high resolution data would be more pronounced when analysing data obtained over a shorter time period.

A detailed analysis of back trajectory sensitivity to the meteorological data resolution under all the different synoptic types is a subject for future studies.

ACKNOWLEDGMENTS

The NOAA Air Resources Laboratory (ARL) made available the HYSPLIT transport and dispersion model and the relevant input files for generation of back trajectories used in this paper. We would also like to thank the Mesoscale and Microscale Meteorology (MMM) Division of NCAR for supporting WRF development.

SUPPLEMENTARY MATERIALS

Supplementary data associated with this article can be found in the online version at http://www.aaqr.org.

REFERENCES

Angevine, W.M., Brioude, J., McKeen, S., Holloway, J.S., Lerner, B.M., Goldstein, A.H., Guha, A., Andrews, A., Nowak, J.B., Evan, S., Fischer, M.L., Gilman, J.B. and Bon, D. (2013). Pollutant Transport among California Regions. *J. Geophys. Res.* 118: 6750–6763.

Begum, B.A., Biswas, S.K., Pandit, G.G., Saradhi, V., Waheed, S., Siddique, N., Seneviratne, M.C.S., Cohen, D.D., Markwitz, A. and Hopke P.K. (2011). Long-range Transport of Soil Dust and Smoke Pollution in the South Asian Region. *Atmos. Pollut. Res.* 2: 151–157.

Bowman, K. P., Lin, J. C., Stohl, A., Draxler, R., Konopka, P., Andrews, A. and Brunner, D. (2013). Input Data Requirements for Lagrangian Trajectory Models. *Bull. Am. Meteorol. Soc.* 94: 1051–1058, doi: 10.1175/BAMS-D-12-00076.1.

Buchanan, C.M., Beverland, I.J. and Heal M.R. (2002). The Influence of Weather-type and Long-range Transport on Airborne Particle Concentrations in Edinburgh, UK. *Atmos. Environ.* 36: 5343–5354.

Charlson, R.J., Schwartz, S.E., Hales, J.M., Cess, R.D., Coakley, J.A., Hansen, J.E. Jr. and Hofmann, D.J. (1992). Climate Forcing by Anthropogenic Aerosols. *Science* 255: 423–430.

Cohen, D.D., Bailey, G.M. and Kondepudi, R. (1996). Elemental Analysis by PIXE and Other IBA Techniques and their Application to Source Fingerprinting of Atmospheric Fine Particle Pollution. *Nucl. Instrum. Methods Phys. Res., Sect. B* 109: 218–226.

Cohen, D.D., Garton, D., Stelcer, E. and Hawes, O. (2004). Accelerator Based Studies of Atmospheric Pollution Processes. *Radiat. Phys. Chem.* 71: 758–567.

Cohen, D.D., Stelcer, E., Garton, D. and Crawford, J. (2011). Fine Particle Characterisation, Source Apportionment and Long-range Dust Transport into the Sydney Basin: A Long Term Study between 1998 and 2009. *Atmos. Pollut. Res.* 2: 182–189.

Cohen, D.D., Crawford, J., Stelcer, E. and Atanacio, A.J. (2012). Application of Positive Matrix Factorization, Multi-linear Engine and Back Trajectory Techniques to the Quantification of Coal-fired Power Station Pollution in Metropolitan Sydney. *Atmos. Environ.* 61: 204–211.

Davis, R.E. and Gay, D.A. (1993). An Assessment of Air Quality Variations in the South-western USA Using an Upper Air Synoptic Climatology. *Int. J. Climatol.* 13: 755–781.

Dayan, U. and Levy, I. (2005). The Influence of Meteorological Conditions and Atmospheric Circulation Types on PM_{10} and Visibility in Tel Aviv. *J. App. Meteorol*. 44: 606–619.

Dockery, D.W., Pope III., C.A., Xiping, X., Spengler, J.D., Ware, J.H., Fay, W.E., Ferris Jr., B.G. and Speiser, F.E. (1993). An Association between Air Pollution and Mortality in Six US Cities. *N. Engl. J. Med.* 329: 1753–1759.

Draxler, R.R. (1987). Sensitivity of a Trajectory Model to the Spatial and Temporal Resolution of the Meteorological Data during CAPTEX. *J. Clim. Appl. Meteorol.* 26: 1577–1588.

Draxler, R.R. and Rolph, G.D. (2003). Hybrid Single-Particle Lagrangian Integrated Trajectory (HYSPLIT), Model. http://www.arl.noaa.gov/ready/hysplit4.html.

Fleming, Z.L., Monks, P.S. and Manning, A.J. (2012). Review: Untangling the Influence of Air-mass History in Interpreting Observed Atmospheric Composition. *Atmos. Res*. 104–105: 1–39.

Hart, M., De Dear, R. and Hyde, R. (2006). A Synoptic Climatology of Tropospheric Ozone Episodes in Sydeny, Australia. *Int. J. Climatol.* 26: 1635–1649.

Hartonen, K., Laitinen, T. and Riekkola, M.L (2011) Current Instrumentation for Aerosol Mass Spectrometry. *TrAC, Trends Anal. Chem.* 30: 1486–1496, doi: 10.1016/j.trac.2011.06.007.

Hawkins, T.W. and Holland, L.A. (2010). Synoptic and Local Weather Conditions Associated with $PM_{2.5}$ Concentration in Carlisle, Pennsylvania. *Middle States Geographer* 43: 72–84.

Huang, X.F, Yu, J.Z, Yuan, Z.B, Lau, A.K.H. and Louie,

P.K.K. (2009). Source Analysis of High Particulate Matter Days in Hong Kong. *Atmos. Environ*. 43: 1196–1203.

Huebert, B.J., Bates, T., Russell, P.B., Shi, G., Kim, Y.J., Kawamura, K., Carmichael, G. and Nakajima, T. (2003). An Overview of ACE-Asia: Strategies for Quantifying the Relationships between Asian Aerosols and their Climatic Impacts. *J. Geophys. Res*. 108: 8633, doi: 10.1029/2003JD003550.

Jiang, N., Hay, J.E. and Fisher, G.W. (2005). Synoptic Weather Patterns and Morning Rush Hour Nitrogen Oxides Concentrations during Auckland Winters. *Weather Clim.* 25: 43–69.

Jiang, N., Cheung, K., Luo, K., Beggs, P.J. and Zhou, W. (2012). On Two Different Objective Procedures for Classifying Synoptic Weather Types over East Australia. International. *J. Climatol.* 32: 1475–1494. doi: 10.1002/joc.2373.

Jiang, N., Betts, A. and Quigley, S. (2013a). Visualisation of Climate and Air Quality Data Using Self-organising Maps. In Proceedings of 21st International Clean Air and Environment Conference (CASANZ), 7–11 September 2013, Sydney. doi: 10.13140/2.1.2285.0244.

Jiang, N., Luo, K., Beggs, P. J., Cheung, K. and Scorgie, Y. (2014). Insights into the Implementation of Synoptic Weather-type Classification Using Self-organizing Maps: an Australian Case Study. *Int. J. Climatol*. 35: 3471–3485, doi: 10.1002/joc.4221.

Jiang, Y., Liu, X., Yang, X.Q. and Wang, M. (2013b). A Numerical Study of the Effect of Different Aerosol Types on East Asian Summer Clouds and Precipitation. *Atmos. Environ.* 70: 51–63.

Kim, J., Yoon, S.C., Jeffeson, A., Zahorowski, W. and Kang, C.H. (2005). Air Mass Characterisation and Source Region Analysis for the Gosan Super-site, Korea, during the ACE-Asia 2001 Field Campaign. *Atmos. Environ*. 39: 6513–6523.

Kohonen, T. (2001). *Self-Organising Maps*. Springer-Verlag, Berlin.

Lai, L.W. (2014). Relationship between Fine Particulate Matter Events with Respect to Synoptic Weather Patterns and the Implications for Circulatory and Respiratory Disease in Taipei, Taiwan. *Int. J. Environ. Health Res*. 24: 528–545, doi: 10.1080/09603123.2013.865717.

Leighton, R.M. and Spark, E. (1997). Relationship between Synoptic Climatology and Pollution Events in Sydney. *Int. J. Biometeorol*. 41: 76–89.

Leśniok, M., Malarzewski, L. and Niedźwiedź, T. (2010). Classification of Circulation Types for Southern Poland with an Application to Air Pollution Concentration in Upper Silesia. *Phys. Chem. Earth* 35: 516–522.

Liu, N., Yu, Y., He, J. and Zhao, S. (2013). Integrated Modelling of Urban-scale Pollutant Transport: Application in a Semi-arid Urban Valley, Northwestern China. *Atmos. Pollut. Res.* 4: 306–314.

Loomis, D. (2000). Sizing up Air Pollution Research. *Epidemiology* 11: 2–4.

McTainsh, G., Chan, Y.C., McGowan, H., Leys, J. and Tews, K. (2005). The 23rd October 2002 Dust Storm in Eastern Australia: Characteristics and Meteorological Conditions. *Atmos. Environ*. 39: 1227–1236.

Moloi, K., Chinidza, S., Selin, Lindgren, E., Viksna, A. and Standzenieks, P. (2002). Black Carbon, Mass and Elemental Measurements of Airborne Particles in the Village of Serowe, Botswana. *Atmos. Environ*. 36: 2447–2457.

NSW (2011). Air pollution – Particulate Matter ($PM_{2.5}$). Office of Environment and Heritage, NSW Government. ISBN 978 1 74293 266 8

Park, M.H. and Kim, Y.P. (2004). Aerosol Composition Change between 1992 and 2002 at Gosan, Korea. *J. Geophys. Res*. 109: D19S13, doi: 10.1029/2003JD004110.

Russell, A.G. and Brunekreef, B. (2009). A Focus on Particulate Matter and Health. *Environ. Sci. Technol.* 43: 4620–4625.

Saha, S., Moorthi, S., Pan, H. L., Wu, X., Wang, J., Nadiga, S., Tripp, P., Kistler, R., Woollen, J. and Behringer, D. (2010). The NCEP Climate Forecast System Reanalysis. *Bull. Am. Meteorol. Soc.* 91: 1015–1057.

Saha, S., Moorthi S., Wu, X., Wang J., Nadig,a S., Tripp, P., Behringer, D., Hou, Y.T., Chuang, H., Iredell, M., Ek, M., Meng, J., Yang, R., Mendez, M. P., van den Dool, H., Zhang, Q., Wang, W., Chen, M. and Becker, E. (2013). The NCEP Climate Forecast System Version 2. *J. Clim*. 27: 2185–2208, doi: 10.1175/JCLI-D-12-00823.1.

Schwarts, J., Dockery, D.W., and Neas, L.M. (1996). Is Daily Mortality Associated Specifically with Fine Particles? *J. Air Waste Manage. Assoc.*46: 927–939.

Seinfeld, J.H. and Pandis, S.N. (1998). Atmospheric Chemistry and Physics. In *From Air Pollution to Climate Change*, John Wiley and Sons, Inc, USA. ISBN 0-471-1-17816-0.

Skamarock, W.C. (2004). Evaluating Mesoscale NWP Models Using Kinetic Energy Spectra. *Mon. Weather Rev.* 132: 3019–3032.

Skamarock, W.C. and Klemp, J.B. (2008). A Time-split Nonhydrostatic Atmospheric Model for Weather Research and Forecasting Applications. *J. Comput. Phys*. 227: 3465–3485, doi: 10.1016/j.jcp.2007.01.037.

USEPA (2007). Guidance on the Use of Models and Other Analyses for Demonstrating Attainment of Air Quality Goals for Ozone, $PM_{2.5}$, and Regional Haze. United States Environmental Protection Agency, EPA-454/B-07-002.

VES (2012). Vehicle Emissions Standards, http://www.infrastructure.gov.au/roads/environment/emission/index.aspx.

Received for review, March 16, 2015
Revised, July 22, 2015
Accepted, August 30, 2015